

# Dynamics of neural fields with exponential temporal kernel

Elham Shamsara · Marius E. Yamakou · Fatihcan  
M. Atay · Jürgen Jost

Received: date / Accepted: date

**Abstract** Various experimental methods of recording the activity of brain tissue in vitro and in vivo demonstrate the existence of traveling waves. Neural field theory offers a theoretical framework within which such phenomena can be studied. The question then is to identify the structural assumptions and the parameter regimes for the emergence of traveling waves in neural fields. In this paper, we consider the standard neural field equation with an exponential temporal kernel. We analyze the time-independent (static) and time-dependent (dynamic) bifurcations of the equilibrium solution and the emerging Spatio-temporal wave patterns. We show that an exponential temporal kernel does not allow static bifurcations such as saddle-node, pitchfork, and in particular, static Turing bifurcations, in contrast to the Green's function used by Atay and Hutt (SIAM J. Appl. Math. 65: 644-666, 2004). However, the exponential temporal kernel possesses the important property that it takes into account the finite memory of past activities of neurons, which the Green's function does not. Through a dynamic bifurcation analysis, we give explicit Hopf (temporally non-constant, but spatially constant solutions) and Turing-Hopf (spatially and temporally non-constant solutions, in particular traveling waves) bifurcation conditions on the parameter space which consists of the coefficient of the exponential temporal kernel, the transmission speed of neural signals, the time delay rate of synapses, and the ratio of excitatory to inhibitory synaptic weights.

**Keywords** Neural fields, exponential temporal kernel, leakage, transmission delays, bifurcation analysis, spatio-temporal patterns

**Mathematics Subject Classification (2010)** 92C20 · 37N25 · 37G10

---

E. Shamsara · M. E. Yamakou · J. Jost

Max-Planck-Institut für Mathematik in den Naturwissenschaften, Inselstr. 22, 04103 Leipzig, Germany

E. Shamsara

Social Determinants of Health Research Center, Mashhad University of Medical Sciences, 91778-99191 Mashhad, Iran

M. E. Yamakou

Angewandte Analysis, Department Mathematik, Friedrich-Alexander-Universität Erlangen-Nürnberg, Cauerstr. 11, 91058 Erlangen, Germany

Fatihcan M. Atay

Department of Mathematics, Bilkent University, 06800 Ankara, Turkey

J. Jost

Santa Fe Institute for the Sciences of Complexity, NM 87501, Santa Fe, USA

E-mail: elham.shamsara@mail.um.ac.ir

E-mail: marius.yamakou@fau.de, Corresponding author

E-mail: f.atay@bilkent.edu.tr

E-mail: jost@mis.mpg.de

## 1 Introduction

It is a well established and basic neurophysiological fact that neural activity leads to particular spatiotemporal patterns in the cortex, see for instance the survey in [1], and other brain structures like the hippocampus, see for example [3]. These spatiotemporal patterns have the qualitative properties of periodic or traveling waves, see for instance [2]. Such patterns, like periodic and traveling waves, play important roles in neurophysiological models of cognitive processing, beginning with the synchronization models of von der Malsburg [4] or the synfire chains of Abeles [5]. It is therefore important to understand the emergence of these patterns in densely connected networks of neurons that communicate with each other by transmitting neural information via their synapses [7]. For understanding such macroscopic patterns, it seems natural to abstract from details at the microscopic, that is, neuronal, level and to study pattern formation from a more general perspective. One recent approach [6] looks at the electromagnetic properties and the folding geometry of brain tissue. A more classical, and by now rather well-established approach is neural field theory. Neural field theory considers populations of neurons embedded in a coarse-grained spatial area and neural field equations describe the spatio-temporal evolution of coarse grained variables like the firing rate activity in these populations of neurons [8]. Neural field models were first introduced by Wilson and Cowan as a spatially extended version of Hopfield neural networks [8, 9]. A simplified model that could be mathematically treated in rather explicit form was developed by Amari [10], which consists of nonlinear integro-differential equations. These equations play an important role also in other fields such as machine learning, which combines ideas from neural field modeling and model based recognition [11, 12].

Neural fields have seen significant progress in both theoretical and numerical studies over the recent years [13–20]. An important fact in neural field modeling is the consideration of axonal conduction delays arising from the finite speed of signals traveling along the axonal distance. Some recent and significant contributions to neural fields modeling with transmission delays are presented in [22–25]. In [22], a stability analysis is given for neural field equations in the presence of finite propagation speed and for a general class of connectivity kernels, and sufficient conditions for the stability of equilibrium solutions are given. It is shown that the non-stationary bifurcations of equilibria depend on the propagation delays and the connectivity kernel, whereas the stationary bifurcations depend only on the connectivity kernel. In [24], the stability of neural fields with a general connectivity kernel and space dependent transmission delays is analyzed. It is found that Turing instability occurs with local inhibition and lateral excitation, while wave instability occurs with local excitation and lateral inhibition. The standard field model of neural populations with propagation speed distribution of signal transmission speeds is considered in [25], where the effect of distributed speeds on the dynamical behavior is investigated. It is shown that the variance of the speed distribution affects the frequency of bifurcating periodic solutions and the phase speed of traveling waves. It is also shown that the axonal speed distributions lead to the increases of the traveling front speed. The results in [25] were extended in [23], where long-range feedback delays are considered in the standard neural field model. There, it is shown that in a reduced model delayed excitatory feedback generally facilitates stationary bifurcations and Turing patterns, while suppressing the bifurcation of periodic solutions and traveling waves. In case of oscillatory bifurcations, the variance of the distributed propagation and feedback delays affects the frequency of periodic solutions and the phase speed of traveling waves.

The objective of this work is to analytically and numerically study the static and dynamic bifurcations and spatio-temporal wave patterns generated by the classical neural field model with an *exponential* temporal kernel. This form of the temporal kernel is more general than the Green's function used in [22] and [26]. In [26] the temporal connectivity kernel is the product of an alpha function and the Heaviside function, which yields a function with the same properties as the Green's

function, and thus yields the same characteristic polynomial as in [22]. We recall that the Green's function  $G(t, t')$  is the solution to  $LG(t, t') = \delta(t-t')$  satisfying the given boundary conditions, where  $L$  is a differential operator. This is a differential equation for  $G$  (or a partial differential equation if we are in more than one dimension), with a very specific source term on the right-and-side: the Dirac delta, which is an on-off function i.e., either 0 if  $t \neq t'$  or  $\infty$  if  $t = t'$ , and hence does not take into account finite memory of past activities of neurons. In contrast, in this paper, the derivative of the exponential temporal kernel tends to 0 as  $t \rightarrow \infty$  and also decreases monotonically in finite time, meaning that it takes into account a finite memory of past activities of neurons, which the Green's function does not. Ref. [26] is quite inspiring for reducing a biologically more realistic microscopic model of leaky integrate-and-fire neurons with distance-dependent connectivity to an effective neural field model. Because of the type of kernels used there, two different neuron populations, excitatory and inhibitory ones, are needed to induce dynamic bifurcations. Here, we work with a Mexican hat type spatial kernel (which models short range excitation and mid range inhibition) and, as explained, an exponential temporal kernel, and we can therefore generate similar types of dynamic bifurcations as in [26] with only a single population.

Thus, in our model, we have excluded the biologically uninteresting static bifurcations, but have produced those, and identified the necessary parameter regimes, for periodic patterns via Hopf bifurcations and, biologically more interestingly, for traveling wave like spatiotemporal patterns via Turing-Hopf bifurcations, that is, precisely those patterns that are typically seen in electrophysiological recordings of the activity of cortical and other brain tissues and that may support basic cognitive processes at the neurophysiological level.

This paper is organized as follows: In Sect. 2, we present the model equation and obtain its equilibrium solution. Sect. 3 is devoted to the static bifurcation analysis of the equilibrium solution. In Sect. 5, we investigate dynamic bifurcations of the equilibrium solution and the ensuing patterns of traveling waves. We conclude with some remarks in In Sect. 6.

## 2 The model and the equilibrium solution

We consider a neural field model represented by an infinite-dimensional dynamical system in the form of an integro-differential equation [27–30], with axonal conduction delay [31–33]. In this equation, the position of a neuron at time  $t$  is given by a spatial variable  $x$ , in the literature usually considered to be continuous in  $\mathbb{R}$  or  $\mathbb{R}^2$ . The state of the neural field,  $v(x, t)$  (membrane potential), evolves according to

$$v(x, t) = \int_{-\infty}^t \kappa(t-s)S(x, s) ds + \int_{-\infty}^t \left[ I_1(x, s) - \frac{1}{\tau}v(x, s) \right] ds. \quad (2.1)$$

Here,  $v(x, t)$  is interpreted as a neural field representing the the local activity of a population of neurons at position  $x$  and time  $t$ , and  $I_1(x, t)$  is an external input current. The first integral converts the incoming pulse activity  $S$  of the neuron at  $x$  into its state by convolution with a temporal kernel (impulse response function)  $\kappa$ . The second integral balances the external input  $I_1$  with a decay or leakage term, with a time constant  $\tau > 0$  arising from the temporal decay rate of synapses. In this paper, we take the past activity of neurons into account for the impulse response using an *exponential* temporal kernel. In [22], such a kernel was taken as the Green's function of a first order differential operator. Here, in order to be able to carry out a detailed bifurcation analysis depending on that kernel, we use a more explicit form, namely an exponential decay:

$$\kappa(t-s) = \begin{cases} \alpha_1 e^{-\alpha_2(t-s)} & \text{if } t-s \geq 0, \\ 0 & \text{if } t-s < 0, \end{cases} \quad (2.2)$$

where  $\alpha_1$  and  $\alpha_2$  are positive constants, with a normalization condition requiring that the integral of the kernel be 1, i.e.  $\alpha_1 = \alpha_2 := \alpha$ . Such kernels are standard in the neuroscience literature and are usually called  $\alpha$ -functions (see e.g. [21]): It is worth noting that even though the exponential kernel used in this work reduces to the kernel used in [22] as  $\alpha \rightarrow \infty$ , our bifurcations cannot, in general, automatically reduce to those in [22]. The presence of a leakage term (which is neglected in [22]), characterized by a temporal decay rate parameter  $\tau > 0$  in our model, does not allow for such a reduction.

The crucial idea in neural field models is that the incoming activity  $S(x, t)$  is obtained by a spatial convolution via an integral with some convolution kernel  $J(x, y)$ , that is,

$$S(x, t) = c \int_{\Omega} J(x, y) F\left(v(y, t - \frac{d(x, y)}{\nu})\right) dy + I_2(x, t). \quad (2.3)$$

Here,  $c > 0$  is some constant that involves various temporal and spatial scales,  $\Omega$  is the spatial domain which is usually taken as  $\mathbb{R}$  or  $\mathbb{R}^2$  in the literature, although other choices, like  $\mathbb{R}^3$  or  $S^2$ , are neuro-biologically plausible and mathematically tractable. The synaptic weight function  $J$  typically describes local excitation–lateral inhibition or local inhibition–lateral excitation. The function  $F$  is a transfer function (for instance a sigmoid or a Heaviside function  $H(v - v_{\text{th}})$ , for some threshold  $v_{\text{th}}$ ; however, later on,  $F$  needs to be smooth),  $I_2(x, t)$  is an internal input current,  $d(x, y)$  is the distance between  $x$  and  $y$  (for instance the Euclidean distance  $|y - x|$ ) and  $\nu > 0$  is the transmission speed of neural signals. Thus, a finite transmission speed introduces a distance-dependent transmission delay, which approaches 0 as  $\nu \rightarrow \infty$ . We also assume a homogeneous field where the connectivity  $J(x, y)$  depends only on the distance  $|y - x|$ , and so we replace  $J(x, y)$  by an even function  $J(y - x)$ . In our numerical investigations we will use the following spatial convolution kernel [24] and sigmoid transfer function [8, 36]:

$$J(y - x) = \frac{a_e}{2} e^{-|y-x|} - \frac{a_i}{2} r e^{-|y-x|r}, \quad (2.4)$$

$$F(v) = \frac{1}{1 + \exp(-1.8(v - 3))}, \quad (2.5)$$

respectively, where  $a_e$  and  $a_i$  respectively denote the excitatory and inhibitory synaptic weights and  $r$  denotes the relation of excitatory and inhibitory spatial ranges [35]. The combination of excitatory and inhibitory axonal networks may yield four different spatial interactions, namely pure excitation (i.e., when  $a_i = 0$ ), pure inhibition (i.e., when  $a_e = 0$ ), local excitation - lateral inhibition (i.e., when  $a_e \neq 0$ ,  $a_i \neq 0$ , and  $r < 1$ ) giving  $J$  a Mexican-hat shape, and local inhibition - lateral excitation (i.e., when  $a_e \neq 0$ ,  $a_i \neq 0$ , and  $r > 1$ , giving  $J$  an inverse Mexican-hat shape.

Differentiating (2.1) with respect to  $t$  yields

$$\frac{d}{dt} v(x, t) = \int_{-\infty}^t \frac{d\kappa(t-s)}{dt} S(x, s) ds - \frac{1}{\tau} v(x, t) + \alpha S(x, t) + I_1(x, t) \quad (2.6)$$

Inserting (2.2) and (2.3) in (2.6) gives

$$\begin{aligned} \frac{d}{dt} v(x, t) = & -\alpha^2 c \int_{-\infty}^t e^{-\alpha(t-s)} \int_{\Omega} J(y-x) F\left(v(y, s - \frac{d(x, y)}{\nu})\right) dy ds - \alpha^2 \int_{-\infty}^t e^{-\alpha(t-s)} I_2(x, s) ds \\ & - \frac{1}{\tau} v(x, t) + \alpha c \int_{\Omega} J(y-x) F\left(v(y, t - \frac{d(x, y)}{\nu})\right) dy + \alpha I_2(x, t) + I_1(x, t). \end{aligned} \quad (2.7)$$

In order to analyze the dynamic behavior of (2.7), we assume a constant internal and external input currents, i.e.  $I_1(x, s) = E$ ,  $I_2(x, s) = I_0$ , and a constant solution

$$v(x, t) = v_0. \quad (2.8)$$

Substituting into (2.7) shows that  $v_0$  satisfies the fixed point equation

$$v_0 + \alpha\tau cF(v_0) \int_{\Omega} J(y-x)dy + \alpha\tau I_0 - \alpha\tau I_0 - \alpha\tau cF(v_0) \int_{\Omega} J(y-x)dy - \tau E = 0, \quad (2.9)$$

which is satisfied by the fixed point (equilibrium solution)

$$v_0 = \tau E. \quad (2.10)$$

The other terms in (2.9) cancel because if  $v$  and  $I_2$  are constant, then so is  $S$ , and hence the first integral in (2.1) is independent of  $t$ .

In the following sections, we study the static and dynamic bifurcations of this equilibrium solution.

### 3 Static bifurcation analysis of the equilibrium solution

For the purpose of this paper, we will consider only one spatial dimension, i.e., we take  $\Omega = \mathbb{R}$ . However, one should note that the results presented in this paper may not automatically translate to higher dimensions (i.e.,  $\Omega = \mathbb{R}^N$ ,  $N \geq 2$ ) where entirely new dynamical behaviors could emerge.

To obtain the parametric region of the stability of the equilibrium solution (2.10), we linearize the integro-differential equation (2.7) around the equilibrium solution  $v_0 = \tau E$ . Let  $w(x, t) = v(x, t) - v_0$ . Then,

$$\begin{aligned} \frac{d}{dt}w(x, t) &= -\alpha^2 c \int_{-\infty}^t e^{-\alpha(t-s)} \int_{-\infty}^{\infty} J(y-x) \left[ F(v_0) + F'(v_0)w(y, s - \frac{d(x, y)}{\nu}) \right] dy ds \\ &\quad - \alpha I_0 - \frac{1}{\tau}w(x, t) - \frac{v_0}{\tau} + \alpha c \int_{-\infty}^{\infty} J(y-x) \left[ F(v_0) + F'(v_0)w(y, t - \frac{d(x, y)}{\nu}) \right] dy + \alpha I_0 + E, \end{aligned} \quad (3.1)$$

which simplifies to

$$\begin{aligned} \frac{d}{dt}w(x, t) &= -\alpha^2 c F'(v_0) \int_{-\infty}^t e^{-\alpha(t-s)} \int_{-\infty}^{\infty} J(y-x) w(y, s - \frac{d(x, y)}{\nu}) dy ds \\ &\quad - \frac{1}{\tau}w(x, t) - \frac{v_0}{\tau} + \alpha c F'(v_0) \int_{-\infty}^{\infty} J(y-x) w(y, t - \frac{d(x, y)}{\nu}) dy + E, \end{aligned} \quad (3.2)$$

where the notation  $F'(v_0)$  denotes  $\frac{dF}{dv}(v_0)$ . To check the stability of the equilibrium solution, we substitute the general Fourier-Laplace ansatz for linear integro-differential equations

$$w(x, t) = e^{\lambda t} e^{ikx}, \quad \lambda \in \mathbb{C}, k \in \mathbb{R}, \quad (3.3)$$

into (3.2) to get

$$\begin{aligned} (\tau\lambda + 1)e^{\lambda t} e^{ikx} &= -\alpha^2 c \tau F'(v_0) \int_{-\infty}^t e^{-\alpha(t-s)} e^{\lambda s} \int_{-\infty}^{\infty} J(y-x) e^{iky} e^{-\lambda \frac{d(x, y)}{\nu}} dy ds \\ &\quad + \alpha c \tau F'(v_0) e^{\lambda t} \int_{-\infty}^{\infty} J(y-x) e^{iky} e^{-\lambda \frac{d(x, y)}{\nu}} dy + \tau E - v_0. \end{aligned} \quad (3.4)$$

From (2.10), we note that  $\tau E - v_0 = 0$  in (3.4). The first integral in (3.4) is independent of  $y$ , so

$$\int_{-\infty}^t e^{-\alpha(t-s)} e^{\lambda s} ds = \frac{1}{\alpha + \lambda} e^{\lambda t}, \quad \alpha + \lambda \neq 0. \quad (3.5)$$

By making a change of variable:  $z = y - x$  in (3.4), and considering  $\lambda \neq -\alpha$ , we obtain the linear variational equation as

$$\tau\lambda + 1 = \alpha\tau F'(v_0) \left( \frac{\lambda}{\alpha + \lambda} \right) \int_{-\infty}^{\infty} J(z) e^{-\lambda \frac{|z|}{\nu}} e^{-ikz} dz. \quad (3.6)$$

Now we define  $L(\lambda)$  as

$$L(\lambda) := \tau\lambda + 1 = \alpha\tau F'(v_0) \left( \frac{\lambda}{\alpha + \lambda} \right) \int_{-\infty}^{\infty} J(z) e^{-\lambda \frac{|z|}{\nu}} e^{-ikz} dz. \quad (3.7)$$

For static bifurcations, that is, for bifurcations leading to temporally constant solutions, we must have  $\lambda = 0$  [22]. However,  $\lambda = 0$  is not a solution of (3.7). And in fact, for a temporal constant  $\neq \tau E$ , the second integral in (2.1) would become infinite. Therefore, static bifurcations (such as saddle-node and pitchfork bifurcations) cannot occur, and hence, in particular, we conclude

**Theorem 1** *The neural field equation (2.1) with an exponential temporal kernel (2.2) does not admit static Turing patterns.*

This is in contrast to the models investigated in [34, 35] where such patterns may occur.

#### 4 A stability condition for a constant equilibrium

We next give a sufficient condition for the asymptotic stability of the equilibrium solution  $v_0$ . We make use of the following lemma from [22].

**Lemma 1** *Let  $L(\lambda)$  be a polynomial whose roots have non-positive real parts. Then  $|L(\sigma + i\omega)| \geq |L(i\omega)|$  for all  $\sigma \geq 0$  and  $\omega \in \mathbb{R}$ .*

*Proof* : See [22]. □

**Theorem 2** *Let  $D := |\beta| \int_{-\infty}^{\infty} |J(z)| dz$ , where  $\beta = \alpha\tau F'(v_0)$ . If*

$$D < \min_{\omega \in \mathbb{R}} |L(i\omega)|, \quad (4.1)$$

*then  $v_0$  is asymptotically stable. In particular, the condition*

$$D < 1 \quad (4.2)$$

*is sufficient for the asymptotic stability of  $v_0$ .*

*Proof* : In the ansatz  $w(x, t) = e^{\lambda t} e^{ikx}$ , let  $\lambda = \sigma + i\omega$ , where  $\sigma$  and  $\omega$  are real numbers. We will prove that  $\sigma < 0$  if (4.1) holds. Suppose by the way of contradiction that (4.1) holds but  $\sigma \geq 0$ . From the definition of  $L(\lambda)$  in (3.7), it follows that

$$\begin{aligned} |L(\sigma + i\omega)| &= |\beta| \left| \frac{\sigma + i\omega}{\alpha + \sigma + i\omega} \right| \left| \int_{-\infty}^{\infty} J(z) e^{-(\sigma + i\omega) \frac{|z|}{\nu}} e^{-ikz} dz \right| \\ &\leq |\beta| \left| \frac{\sigma + i\omega}{\alpha + \sigma + i\omega} \right| \int_{-\infty}^{\infty} |J(z)| \left| e^{-(\sigma + i\omega) \frac{|z|}{\nu}} \right| dz \\ &\leq |\beta| \left| \frac{\sigma + i\omega}{\alpha + \sigma + i\omega} \right| \int_{-\infty}^{\infty} |J(z)| dz. \end{aligned}$$

Since  $\alpha > 0$ , we have  $\left| \frac{\sigma + i\omega}{\alpha + \sigma + i\omega} \right| < 1$ , which means

$$|L(\sigma + i\omega)| < |\beta| \int_{-\infty}^{\infty} |J(z)| dz. \quad (4.3)$$

By Lemma 1,

$$|L(i\omega)| \leq |L(\sigma + i\omega)| < |\beta| \int_{-\infty}^{\infty} |J(z)| dz =: D, \quad (4.4)$$

for some  $\omega \in \mathbb{R}$ . This, however, contradicts (4.1). Thus  $\sigma < 0$ , and the equilibrium solution  $v_0$  is asymptotically stable. This proves the first statement of the theorem. From the definition of  $L(\lambda)$  in (3.7), one has  $|L(i\omega)|^2 = 1 + \tau^2\omega^2$ . Hence, if (4.2) is satisfied, then

$$D^2 < 1 \leq 1 + \tau^2\omega^2 = |L(i\omega)|^2 \quad (4.5)$$

for all  $\omega \in \mathbb{R}$ , which is a sufficient condition for stability by (4.2).  $\square$

In Fig.1(a)-(c), we present the bifurcation diagrams showing the regions of stability and instability of the equilibrium solution  $v_0$ . In the panels, the quantity  $D := |\beta| \int_{-\infty}^{\infty} |J(z)| dz$  is plotted against the bifurcation parameters  $\alpha$ ,  $r$ , and  $\tau$ .

We are interested in parameter constellations where spatiotemporal patterns emerge, that is, where the constant solution is *not* stable. From the diagrams we see that this requires that the memory decay  $\alpha$  and the time constant  $\tau$  of the synapses both be large enough and that excitation and inhibition need to be sufficiently imbalanced. In fact, the case  $r < 1$ , where inhibition is weaker, but more widely spread than excitation, is usually assumed in the literature to let  $J$  acquire its Mexican hat shape.

## 5 Dynamic bifurcation analysis of the equilibrium solution

In Section 3, we have seen that static bifurcations are not possible since  $\lambda = 0$  is not a solution of (3.7). In this section, we investigate the conditions for oscillatory (dynamic) bifurcations. In case of a homogeneous neural field, we use the kernel function  $J$  and the sigmoid transfer function  $F$  in (2.4) and (2.5), respectively. Equation (3.7), which an infinitesimal perturbation  $w(x, t) = e^{\lambda t} e^{ikx}$  needs to satisfy, can then be written as

$$\begin{aligned} \tau\lambda^2 + (\tau\alpha + 1)\lambda + \alpha &= \alpha c \tau F'(v_0) \lambda \int_{-\infty}^{\infty} J(z) e^{-\lambda \frac{|z|}{\nu}} e^{-ikz} dz \\ &= \beta \lambda \left[ \int_{-\infty}^{\infty} \left( \frac{a_e}{2} e^{-|z|} - \frac{a_i r}{2} e^{-|z|r} \right) e^{-\lambda \frac{|z|}{\nu}} e^{-ikz} dz \right] \\ &= \beta \lambda \left[ a_e \frac{1}{\left(1 + \frac{\lambda}{\nu}\right) + ik} - a_i r \frac{1}{\left(r + \frac{\lambda}{\nu}\right) + ik} \right] \\ &= \beta \lambda \left[ a_e \frac{1 + \frac{\lambda}{\nu}}{\left(1 + \frac{\lambda}{\nu}\right)^2 + k^2} - a_i r \frac{r + \frac{\lambda}{\nu}}{\left(r + \frac{\lambda}{\nu}\right)^2 + k^2} \right] \\ &\quad - i\beta \lambda k \left[ \frac{a_e}{\left(1 + \frac{\lambda}{\nu}\right)^2 + k^2} - \frac{a_i r}{\left(r + \frac{\lambda}{\nu}\right)^2 + k^2} \right]. \end{aligned} \quad (5.1)$$

Comparing the real parts of the two sides of (5.1), we get

$$\begin{aligned} &\left[ k^2 + \left( r + \frac{\lambda}{\nu} \right)^2 \right] \left[ k^2 + \left( 1 + \frac{\lambda}{\nu} \right)^2 \right] \left( \tau\lambda^2 + (\tau\alpha + 1)\lambda + \alpha \right) \\ &\quad - a_e \beta \lambda \left( 1 + \frac{\lambda}{\nu} \right) \left[ k^2 + \left( r + \frac{\lambda}{\nu} \right)^2 \right] + r a_i \beta \lambda \left( r + \frac{\lambda}{\nu} \right) \left[ k^2 + \left( 1 + \frac{\lambda}{\nu} \right)^2 \right] = 0, \end{aligned} \quad (5.2)$$

which is a polynomial of degree six in  $\lambda$ . We consider the solutions  $\lambda$  as functions of  $k$ . The solution loses its asymptotic stability when we find a solution with  $\text{Re}\lambda > 0$ . By tuning the parameters  $r$ ,

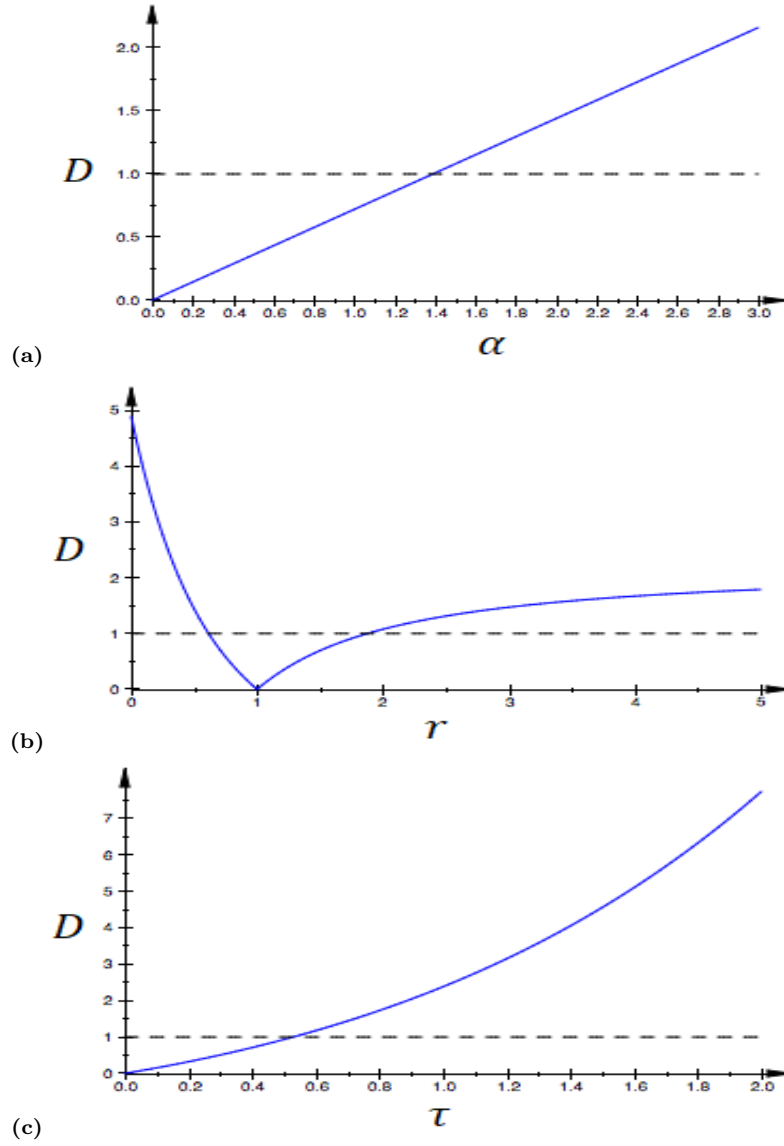


Figure 1: The blue curves represent the quantity  $D$  from Theorem 2 plotted against the bifurcation parameters:  $\alpha$  in (a) with  $\tau = 0.7$ ,  $r = 0.5$ ;  $r$  in (b) with  $\alpha = 2.0$ ,  $\tau = 0.7$ ; and  $\tau$  in (c) with  $\alpha = 2.0$ ,  $r = 0.5$ . The intervals of  $\alpha \in (0.0, 1.4)$ ,  $r \in (0.60, 1.84)$ , and  $\tau \in (0.0, 0.51)$  in which the blue curves are below the dashed horizontal line fulfill the sufficient condition of asymptotic stability of the equilibrium solution  $v_0 = \tau E$ , following Theorem 2. Other parameters are fixed at:  $c = 15.0$ ,  $E = 0.275$ ,  $a_e = 10.0$ ,  $a_i = a_e/r$ . The nonlinear dependence on  $\tau$ , as opposed to the linear dependence on  $\alpha$ , arises because in  $\beta = \alpha c \tau F'(v_0)$ , we get an additional dependence since  $v_0 = \tau E$ .

$\tau$  or  $\alpha$ , a critical point is eventually reached at  $k = k_c$  in which the real part of the corresponding eigenvalue  $\lambda(k_c)$  of (5.2) becomes zero. From this critical point, one gets the critical wave-number  $k_c$  and the critical frequency  $\omega_c = \text{Im} \lambda(k_c)$ . The case  $k_c = 0$  and  $\omega_c \neq 0$  corresponds to a Hopf bifurcation [37–39], and the case  $k_c \neq 0$  and  $\omega_c \neq 0$  to a Turing-Hopf bifurcation [34, 40, 41]. We shall investigate both cases in more detail.

### 5.1 Hopf bifurcation

We search for conditions for Hopf bifurcation, i.e., when  $k_c = 0$  and the real part of the corresponding eigenvalue  $\lambda|_{(k_c=0)}$  becomes zero, while  $\omega_c = \text{Im } \lambda|_{(k_c=0)} \neq 0$ . To obtain these conditions, we insert  $k = k_c = 0$  in (5.2) and obtain

$$q_6\lambda^6 + q_5\lambda^5 + q_4\lambda^4 + q_3\lambda^3 + q_2\lambda^2 + q_1\lambda + q_0 = 0, \quad (5.3)$$

where

$$\begin{cases} q_6 = \tau, \\ q_5 = 2\tau(r+1)\nu + \alpha\tau + 1, \\ q_4 = 2\tau(0.5 + 0.5r^2 + 2r)\nu^2 + ((a_i\beta + 2\alpha\tau + 2)r + 2\alpha\tau - a_e\beta + 2)\nu + \alpha, \\ q_3 = 2\tau(r+1)r\nu^3 + [(\alpha\tau + a_i\beta + 1)r^2 + 4(\alpha\tau + 1 - (a_e - a_i)\beta)r \\ + \alpha\tau + 1 - a_e\beta]\nu^2 + 2\alpha(r+1)\nu, \\ q_2 = \tau r^2\nu^4 + [(2\alpha\tau + 2 - (a_e - 2a_i)\beta)r^2 + (2\alpha\tau + 2 + (-2a_e + a_i)\beta)r]\nu^3 \\ + \alpha(1 + r^2 + 4r)\nu^2, \\ q_1 = (\alpha\tau + 1 - (a_e - a_i)\beta)r^2\nu^4 + 2\alpha(r+1)r\nu^3, \\ q_0 = \alpha\nu^4r^2. \end{cases} \quad (5.4)$$

By simplifying (5.3), one can already get two of its six solutions, given by

$$\begin{cases} \lambda_1 = -\nu, \\ \lambda_2 = -\nu r. \end{cases} \quad (5.5)$$

The remaining four solutions of (5.3) should then satisfy the polynomial equation of degree four:

$$p_4\lambda^4 + p_3\lambda^3 + p_2\lambda^2 + p_1\lambda + p_0 = 0, \quad (5.6)$$

where

$$\begin{cases} p_4 = \tau, \\ p_3 = \tau\nu r + \alpha\tau + \tau\nu + 1, \\ p_2 = \nu a_i\beta r + \nu\alpha r\tau + \tau\nu^2 r - \nu a_e\beta + \nu\alpha\tau + \alpha + (r+1)\nu, \\ p_1 = -a_e\beta\nu^2 r + a_i\beta\nu^2 r + \alpha\nu^2 r\tau + \alpha\nu r + \nu^2 r + \alpha\nu, \\ p_0 = \alpha\nu^2 r. \end{cases} \quad (5.7)$$

Substituting  $\lambda = i\omega_c$  in (5.6) and separating the real and imaginary parts yields

$$\begin{cases} a_4\omega_c^4 + a_2\omega_c^2 + a_0 = 0, \\ b_3\omega_c^3 + b_1\omega_c = 0, \end{cases} \quad (5.8)$$

where

$$\begin{cases} a_4 = \tau, \\ a_2 = -\nu a_i\beta r - \nu\alpha r\tau - \tau\nu^2 r + \nu a_e\beta - \nu\alpha\tau - \alpha - (r+1)\nu, \\ a_0 = \alpha\nu^2 r, \\ b_3 = -\tau\nu r - \alpha\tau - \tau\nu - 1, \\ b_1 = -a_e\beta\nu^2 r + a_i\beta\nu^2 r + \alpha\nu^2 r\tau + \alpha\nu r + \nu^2 r + \alpha\nu. \end{cases} \quad (5.9)$$

We obtain  $\omega_c$  from the second equation of (5.8) as

$$\omega_c^2 = -\frac{b_1}{b_3}. \quad (5.10)$$

Substituting (5.10) in the first equation of (5.8) gives  $\nu = \nu(r, \tau, \alpha, \beta, a_e, a_i)$  as

$$g(\nu) := \nu^4 + \frac{u_3}{u_4}\nu^3 + \frac{u_2}{u_4}\nu^2 + \frac{u_1}{u_4}\nu + \frac{u_0}{u_4} = 0, \quad (5.11)$$

where

$$\begin{cases} u_4 = r^2\tau^2(r+1)(\alpha\tau+1-\beta(a_e-a_i)), \\ u_3 = \tau((\alpha\tau+a_i\beta+1)r^3+(2\alpha\tau+2)r^2+(-a_e\beta+\alpha\tau+1)r)(\alpha\tau-\beta(a_e-a_i)+1), \\ u_2 = (\alpha\tau(a_i\beta+\alpha\tau+1)r^3+(a_i\beta+\alpha\tau+1)(\tau^2\alpha^2-(-3+(a_e-a_i)\beta)\alpha\tau+1+(-a_e+a_i)\beta)r^2 \\ \quad +(-a_e\beta+\alpha\tau+1)(\tau^2\alpha^2-(-3+(a_e-a_i)\beta)\alpha\tau+1+(-a_e+a_i)\beta)r+\alpha\tau(-a_e\beta+\alpha\tau+1)), \\ u_1 = \alpha(\alpha\tau+1)((a_i\beta+\alpha\tau+1)r^2+(2\alpha\tau+2+(-2a_e+2a_i)\beta)r+\alpha\tau-a_e\beta+1), \\ u_0 = \alpha^2(\alpha\tau+1)(r+1). \end{cases} \quad (5.12)$$

**Proposition 1** *If  $(\alpha\tau+1-\beta(a_e-a_i)) < 0$ , then (5.11) has at least one positive root.*

*Proof :* We have  $u_0 > 0$  which implies that  $g(0) = \frac{u_0}{u_4} < 0$  whenever  $(\alpha\tau+1-\beta(a_e-a_i)) < 0$ . And since  $\lim_{\nu \rightarrow \infty} g(\nu) = +\infty$ , then by the continuity of  $g$ , there exists a  $\nu_0$  in  $(0, \infty)$  such that  $g(\nu_0) = 0$ .  $\square$

From (5.9), since we have  $b_3 < 0$ ,  $b_1$  must be positive, so that the right hand side of (5.10) is positive. The positivity of  $b_1$  implies that

$$\nu[\beta(a_e-a_i)-(\alpha\tau+1)] < \frac{\alpha(1+r)}{r}.$$

If  $[\alpha\tau+1-\beta(a_e-a_i)] < 0$ , then  $[\beta(a_e-a_i)-(\alpha\tau+1)] > 0$ , which ensures that

$$\nu < \frac{\alpha(1+r)}{r[\beta(a_e-a_i)-(\alpha\tau+1)]}. \quad (5.13)$$

The positive solutions of (5.11) correspond to the substitution of the values of  $\omega_c$  from (5.10). Thus, at the positive solutions, the Hopf bifurcation occurs in the parametric region satisfying (5.13). In other words, the relation in (5.13) provides the parametric region in which a Hopf bifurcation occurs if the value of  $\omega_c$  in (5.10) also satisfies the first equation in (5.8). The theoretical analysis provides us with infinitesimal conditions for the emergence of periodic solutions. The parameter values of  $\beta$ ,  $a_e$ ,  $a_i$ ,  $\alpha$ , and  $\tau$  are chosen such that  $\beta(a_e-a_i)-(\alpha\tau+1) > 0$ .

In Fig.2, for example, we fix the parameters  $a_e = 10.0$ ,  $a_i = 2.0$ , so that  $r = a_e/a_i$ , and  $c = 15.0$ . We compute the range of values of the bifurcation parameters  $\alpha$  and  $\tau$  for which  $\beta(a_e-a_i)-(\alpha\tau+1) > 0$ . Fig.2(a) and (b) show that  $\beta(a_e-a_i)-(\alpha\tau+1) > 0$  if  $\alpha \in (3.35, 8.0)$  and  $\tau \in (0.54, 2.0)$ , respectively. In Fig.2(c)-(e), the gray area represents the region of the parameter spaces where (5.13) holds. The parts of blue curves that lie in the gray region represent the Hopf bifurcation curves because they satisfy (5.13) and (5.11) simultaneously. We observe that the vertical boundary of the gray region in Fig.2(c) and (d) exactly corresponds to the minimum value of  $\alpha$  and  $\tau$  in Fig.2(a) and (b) where  $\beta(a_e-a_i)-(\alpha\tau+1) > 0$ , respectively. Fig.3(a)-(d) display the space-time patterns of the membrane potential  $v(x, t)$  with parameters chosen from three regions of Fig.2(c). We note that the colorbars of Fig.3(a) and (b) have been rescaled to that of Fig.3(c) and (d), for a better comparison of the amplitudes of the space-time patterns.

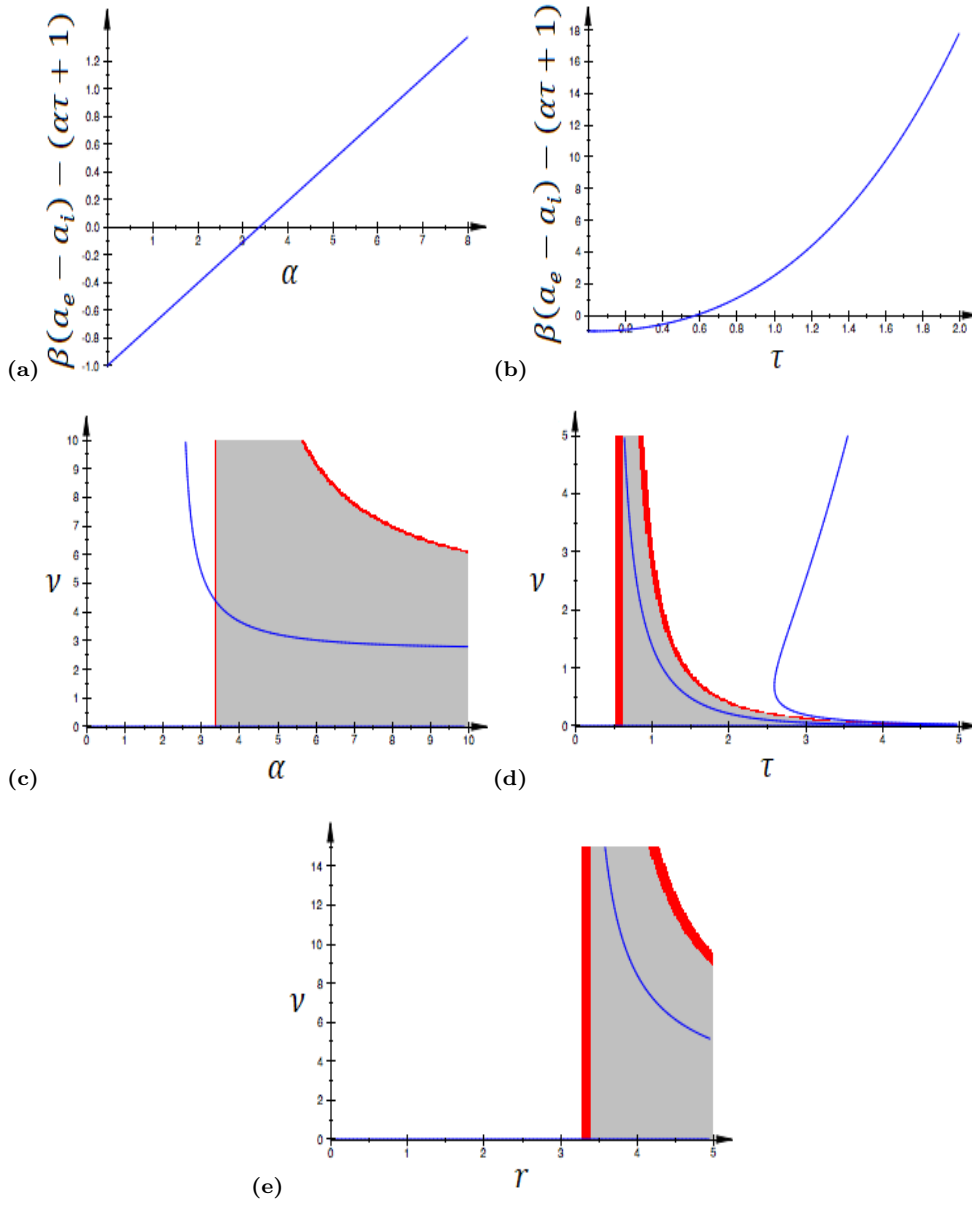


Figure 2: Panels (a) and (b) show that interval of  $\alpha \in (3.35, 8.0)$  and  $\tau \in (0.54, 2.0)$  for which  $\beta(a_e - a_i) - (\alpha\tau + 1) > 0$ , respectively. In the panels (c)-(e), the blue curves represent the solutions of (5.11) in the parameter spaces  $\alpha$ - $\nu$ ,  $\tau$ - $\nu$ , and  $r$ - $\nu$ , respectively. The gray areas represent the region of the parameter spaces where (5.13) holds. The parts of blue curves that lie in the gray region represent the Hopf bifurcation curves because they satisfy (5.13) and (5.11) simultaneously. In (a)  $\tau = 0.75$ ,  $r = 5.0$ ; in (b)  $\alpha = 6.0$ ,  $r = 5.0$ ; in (c)  $\tau = 0.75$ ,  $r = 5.0$ ; in (d)  $\alpha = 6.0$ ,  $r = 5.0$ ; and in (e)  $\alpha = 6.0$ ,  $\tau = 0.75$ . In (a)-(e), the other parameter values are:  $c = 15.0$ ,  $E = 0.275$ ,  $a_e = 10.0$ ,  $v_0 = \tau E$ ,  $\beta = \alpha c \tau F'(v_0)$ , and in (e)  $a_i = a_e/r$ .

When the parameter values are chosen on or above the blue curve in the gray region where  $\beta(a_e - a_i) - (\alpha\tau + 1) > 0$ , the neural field always have stable periodic solutions with a relatively large amplitude of approximately 0.592. In Fig.3(a), the parameters are chosen in the white region, where  $\beta(a_e - a_i) - (\alpha\tau + 1) < 0$ , and there are no oscillations as  $v(x, t)$  stays constant around 0.017. In Fig.3(b), the parameters are chosen in the gray region, where  $\beta(a_e - a_i) - (\alpha\tau + 1) > 0$ , and below the blue Hopf bifurcation curve. Here, the voltage  $v(x, t)$  oscillates with a small amplitude of 0.325 and a temporal frequency of 15 oscillations per 50 time units. In Fig.3(c), the parameters are chosen in the gray region, where  $\beta(a_e - a_i) - (\alpha\tau + 1) > 0$  but exactly on the blue Hopf bifurcation curve. Here, the voltage  $v(x, t)$  oscillates with a larger amplitude of 0.592 (with 16 oscillations per 50 time units) compared to 0.325 (with 15 oscillations per 50 time units) in Fig.3(b). This makes sense because as we get closer to the blue curve, we in fact get closer to the Hopf bifurcation threshold and hence the amplitude of oscillations gets bigger. In Fig.3(d), the parameters are still chosen in the gray region, where  $\beta(a_e - a_i) - (\alpha\tau + 1) > 0$  but above the blue Hopf bifurcation curve and the oscillations of the voltage  $v(x, t)$  persist with an amplitude 0.538 and a higher frequency (29 oscillations per 50 time units) of oscillation than Fig.3(b) and Fig.3(c).

Thus, when  $\alpha$  (the parameter of the exponential kernel in (2.2)) and  $\nu$  (the transmission speed of the nerve impulse) increase, in the Hopf bifurcation region, the amplitude and frequency of oscillations of the membrane potential also increase. When  $\alpha$  increases, the internal states of neurons decay faster, and they become more receptive to external input, and when the transmission speed  $\nu$  increases, signals can travel faster, and therefore also oscillations can speed up.

## 5.2 Turing-Hopf bifurcation

**Theorem 3** *The neural field equation (2.1) admits a Turing-Hopf bifurcation when the set of parameters  $\{\alpha, \nu, \tau, r, a_e, a_i\}$  satisfies*

$$\begin{aligned} & \frac{\tau}{\nu^2} \left( \frac{r^2 a_e - a_i}{r^2} \right) \omega^4 + \left[ \tau(a_i - a_e) + \left( \tau k^2 - \frac{\alpha}{\nu^2} \right) \left( \frac{r^2 a_e - a_i}{r^2} \right) + \left( \frac{\alpha\tau + 1}{\nu} \right) \left( \frac{r a_e - a_i}{r} \right) \right] \omega^2 \\ & + \alpha \left( (a_e - a_i) - k^2 \left( \frac{r^2 a_e - a_i}{r^2} \right) \right) = 0, \end{aligned} \quad (5.14)$$

with  $k \neq 0$  and  $\omega \neq 0$ .

*Proof* The conditions for Turing-Hopf bifurcation require that with the Fourier-Laplace ansatz (3.3), that is,  $w(x, t) = e^{\lambda t} e^{ikx}$ , we find  $\lambda = \pm i\omega$  with  $\omega \neq 0$  at some critical value  $k_c \neq 0$ . Inserting  $\lambda = i\omega$  in (3.7), we obtain

$$L(i\omega) := 1 + i\tau\omega = \beta \left( \frac{i\omega}{\alpha + i\omega} \right) \int_{-\infty}^{\infty} J(z) e^{-i\omega \frac{|z|}{\nu}} e^{ikz} dz, \quad (5.15)$$

which yields upon expansion,

$$\begin{aligned} \beta \frac{\omega^2 + i\alpha\omega}{\alpha^2 + \omega^2} \int_{-\infty}^{\infty} J(z) e^{-\frac{i\omega|z|}{\nu}} \cos(kz) dz &= \beta \frac{\omega^2 + i\alpha\omega}{\alpha^2 + \omega^2} \int_{-\infty}^{\infty} J(z) \left[ \cos\left(\frac{\omega|z|}{\nu}\right) - i \sin\left(\frac{\omega|z|}{\nu}\right) \right] \cos(kz) dz \\ &= \frac{\beta}{2} \frac{\omega^2 + i\alpha\omega}{\alpha^2 + \omega^2} \int_{-\infty}^{\infty} J(z) \left[ \cos\left(\frac{\omega|z|}{\nu} + k|z|\right) + \cos\left(\frac{\omega|z|}{\nu} - k|z|\right) \right] dz \\ &\quad - \frac{i\beta}{2} \frac{\omega^2 + i\alpha\omega}{\alpha^2 + \omega^2} \int_{-\infty}^{\infty} J(z) \left[ \sin\left(\frac{\omega|z|}{\nu} + k|z|\right) + \sin\left(\frac{\omega|z|}{\nu} - k|z|\right) \right] dz \\ &= \frac{\beta}{2} \frac{\omega^2 + i\alpha\omega}{\alpha^2 + \omega^2} \int_{-\infty}^{\infty} J(z) \left[ e^{i|z|(\frac{\omega}{\nu} + k)} + e^{i|z|(\frac{\omega}{\nu} - k)} \right] dz. \end{aligned} \quad (5.16)$$

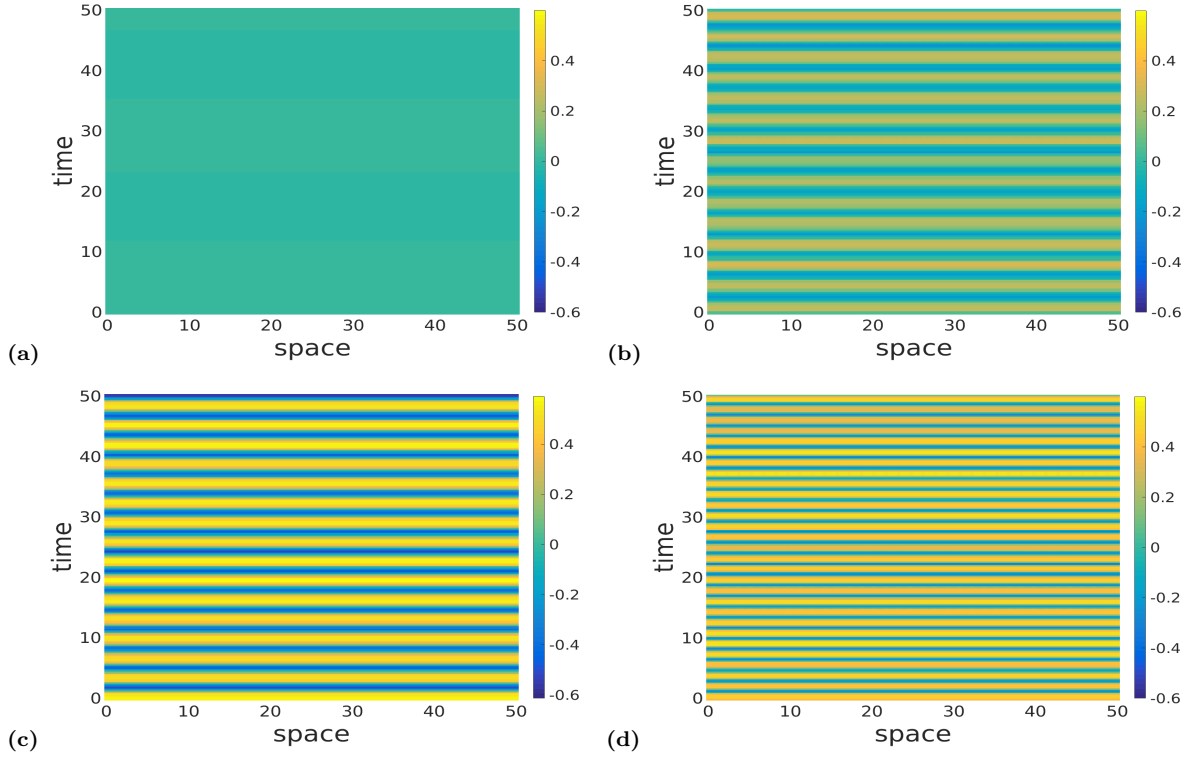


Figure 3: Panels **(a)**-**(d)** show color coded space-time patterns of membrane potential  $v(x, t)$  emerging from Hopf instability. In **(a)**,  $\alpha = 0.1$ ,  $\nu = 0.25$ ,  $\tau = 0.75$ , i.e., out of the gray Hopf bifurcation region ( $\beta(a_e - a_i) - (\alpha\tau + 1) < 0$ ) and there are no oscillations. In **(b)**,  $\alpha = 4.0$ ,  $\nu = 1.0$ ,  $\tau = 0.75$ , i.e., in the gray Hopf bifurcation region ( $\beta(a_e - a_i) - (\alpha\tau + 1) > 0$ ) and *below* the blue Hopf bifurcation curve. Here we have sub-threshold periodic oscillations of a spatially constant solution. In **(c)**,  $\alpha = 6.0$ ,  $\nu = 3.0$ ,  $\tau = 0.75$ , i.e., in the gray Hopf bifurcation region and *exactly on* the blue Hopf bifurcation curve. Here we have supra-threshold periodic oscillations of spatially constant solutions. In **(d)**,  $\alpha = 6.0$ ,  $\nu = 7.0$ ,  $\tau = 0.75$ , i.e., in the Hopf bifurcation region and *above* the blue Hopf bifurcation curve. Here we have a higher frequency supra-threshold periodic oscillations of spatially constant solutions. In all panels, the solutions are obtained for the Gaussian connectivity kernel, with initial conditions chosen randomly from a uniform distribution on  $[v_0 - 0.1, v_0 + 0.1]$ . Other parameters are fixed at  $a_e = 10.0$ ,  $a_i = 2.0$ ,  $r = a_e/a_i = 5.0$ ,  $c = 15.0$ , and  $k = 0$ .

By substituting the power series

$$e^{i|z|(\frac{\omega}{\nu} \pm k)} = \sum_{n=0}^{\infty} \frac{i^n (\frac{\omega}{\nu} \pm k)^n}{n!} |z|^n,$$

(5.16) is written as

$$\frac{\beta \omega^2 + i\alpha\omega}{2 \alpha^2 + \omega^2} \int_{-\infty}^{\infty} J(z) \sum_{n=0}^{\infty} \frac{i^n}{n!} \left[ \left( \frac{\omega}{\nu} + k \right)^n + \left( \frac{\omega}{\nu} - k \right)^n \right] |z|^n dz. \quad (5.17)$$

We define  $J_n$  as

$$J_n := \int_{-\infty}^{\infty} J(z) |z|^n dz. \quad (5.18)$$

Substituting (5.18) into (5.17) yields

$$L(i\omega) = \beta \frac{\omega^2 + i\alpha\omega}{\alpha^2 + \omega^2} \left[ J_0 + i\frac{\omega}{\nu} J_1 - \frac{1}{2!} \left( k^2 + \frac{\omega^2}{\nu^2} \right) J_2 + \dots \right]. \quad (5.19)$$

Equating the right-hand side of (5.19) to the left-hand side of (5.15), we get

$$1 + i\tau\omega = \beta \frac{\omega^2 + i\alpha\omega}{\alpha^2 + \omega^2} \left[ J_0 + i\frac{\omega}{\nu} J_1 - \frac{1}{2!} \left( k^2 + \frac{\omega^2}{\nu^2} \right) J_2 + \dots \right]. \quad (5.20)$$

Equating the real parts of both sides in (5.20), and similarly with the imaginary parts, and considering  $\omega \neq 0$  (a Turing-Hopf bifurcation condition), we have

$$\begin{cases} 1 = \frac{\beta}{\alpha^2 + \omega^2} \left[ \omega^2 J_0 - \alpha\omega \left( \frac{\omega}{\nu} J_1 \right) - \omega^2 \frac{1}{2!} \left( k^2 + \frac{\omega^2}{\nu^2} \right) J_2 + \dots \right], \\ \tau = \frac{\beta}{\alpha^2 + \omega^2} \left[ \alpha J_0 + \omega \left( \frac{\omega}{\nu} J_1 \right) - \frac{1}{2!} \alpha \left( \left( k^2 + \frac{\omega^2}{\nu^2} \right) J_2 \right) + \dots \right]. \end{cases} \quad (5.21)$$

From (5.21) we have

$$\frac{\tau}{\alpha J_0 + \frac{\omega^2}{\nu} J_1 - \frac{\alpha}{2} \left( k^2 + \frac{\omega^2}{\nu^2} \right) J_2} = \frac{\beta}{\alpha^2 + \omega^2} = \frac{1}{\omega^2 J_0 - \alpha \frac{\omega^2}{\nu} J_1 - \frac{\omega^2}{2} \left( k^2 + \frac{\omega^2}{\nu^2} \right) J_2}, \quad (5.22)$$

which gives

$$\alpha J_0 + \frac{\omega^2}{\nu} J_1 - \frac{\alpha}{2} \left( k^2 + \frac{\omega^2}{\nu^2} \right) J_2 = \tau \omega^2 J_0 - \tau \alpha \frac{\omega^2}{\nu} J_1 - \tau \frac{\omega^2}{2} \left( k^2 + \frac{\omega^2}{\nu^2} \right) J_2. \quad (5.23)$$

After substituting (2.4) into (5.18), the convergent improper integrals  $J_n$  ( $n = 0, 1, 2$ ) are calculated and explicitly given as

$$\begin{aligned} J_0 &= -a_i + a_e, \\ J_1 &= \frac{ra_e - a_i}{r}, \\ J_2 &= \frac{2(r^2 a_e - a_i)}{r^2}. \end{aligned} \quad (5.24)$$

Substituting (5.24) into (5.23), we obtain

$$\begin{aligned} & \frac{\tau}{\nu^2} \left( \frac{r^2 a_e - a_i}{r^2} \right) \omega^4 + \left[ \tau(a_i - a_e) + \left( \tau k^2 - \frac{\alpha}{\nu^2} \right) \left( \frac{r^2 a_e - a_i}{r^2} \right) + \left( \frac{\alpha\tau + 1}{\nu} \right) \left( \frac{ra_e - a_i}{r} \right) \right] \omega^2 \\ & + \alpha \left( (a_e - a_i) - k^2 \left( \frac{r^2 a_e - a_i}{r^2} \right) \right) = 0. \end{aligned} \quad (5.25)$$

Thus, (5.25) represents the Turing-Hopf bifurcation in the parameter space  $(\alpha, \nu, \tau, r, a_e, a_i)$  with  $k \neq$  and  $\omega \neq 0$ .  $\square$

Fig.4 shows the dispersion relation of the neural field at fixed values of the other parameters. Here, we arbitrarily fixed the other parameters  $\alpha, \nu, \tau, r, a_e, a_i$  to specific values, and numerically find the corresponding dispersion relation (i.e., the  $k - \omega$  curve) that emerges from the Turing-Hopf equation in (5.25). It can be seen that for one specific value of the spatial mode, i.e.,  $k = 0.897$ , we have several values of the temporal mode, i.e.,  $\omega \in (0.0, 0.5]$ , that satisfy the Turing-Hopf bifurcation equation in (5.25). On the other hand, for one specific value of the temporal mode, i.e.,  $\omega = 2.573$ , we have several values of the spatial mode, i.e., for  $k \in (6.0, 50.0]$ , that satisfy the Turing-Hopf

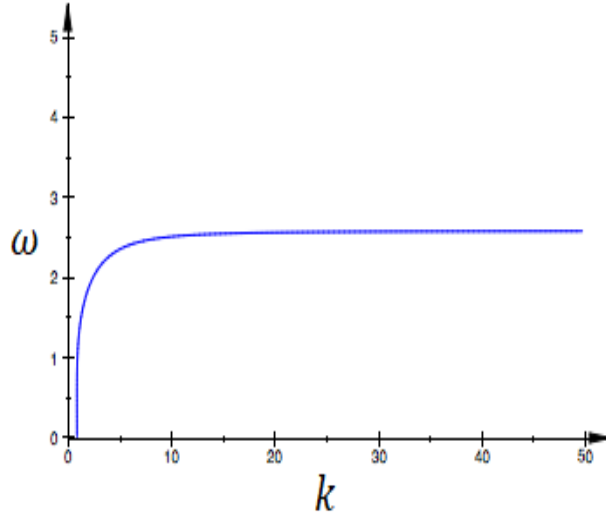


Figure 4: The dispersion relation of the neural field satisfying the Turing-Hopf bifurcation equation given by (5.25). Arbitrarily fixing the parameters at  $\alpha = 5.0$ ,  $\nu = 1.0$ ,  $\tau = 0.75$ ,  $r = 5.0$ ,  $a_e = 10.0$ ,  $a_i = a_e/r = 2.0$ , we can see that for the temporal mode  $\omega \in (0.0, 0.5]$ , only one value of the spatial mode, i.e.  $k = 0.897$ , satisfies this Turing-Hopf bifurcation equation. For  $k \in (6.0, 50.0]$ , only one value of  $\omega$ , i.e.,  $\omega = 2.573$ , satisfies the Turing-Hopf bifurcation curve.

bifurcation equation in (5.25). But, for  $\omega \in (0.5, 2.573)$  and  $k \in (0.897, 6.0]$ , only one pair of values of the spatial and temporal modes satisfies the Turing-Hopf bifurcation equation in (5.25).

In Fig.5(a)-(d), we respectively show the Turing-Hopf bifurcation curves in different parameter spaces:  $(\alpha-\omega)$ ,  $(\nu-\omega)$ ,  $(\tau-\omega)$ , and  $(r-\omega)$ . In Fig.5(a), we used one of the values of the spatial mode (i.e.,  $k = 25.0$ ) for which (5.25) has a unique temporal mode solution (i.e.,  $\omega = 2.573$ ) according to the dispersion relation curve in Fig.4. And in Fig.5(b)-(d), we used a unique value of the spatial mode (i.e.,  $k = 1.0$ ) for which the dispersion relation admits a unique temporal mode solution (i.e.,  $\omega = 0.1$ ). We note the memory decay  $\alpha$  and the leakage parameter  $\tau$  have opposite effects. The first increases the frequency of the oscillations at the bifurcation point, whereas the latter decreases them. The transmission speed has a nonmonotonic influence, with a minimum for  $\omega$  at a particular value of  $\nu$ .

In Fig.6, we display the space-time patterns in three distinct regions of the Turing-Hopf bifurcation curve of Fig.5(a), for example. Here, one can see, as expected, that the Turing-Hopf bifurcation leads to spatially and temporally non-constant solutions. With values fixed at  $k = 25.0$ ,  $\nu = 1.0$ ,  $\tau = 0.75$ ,  $r = 5.0$ ,  $a_e = 10.0$ , and  $a_i = a_e/r = 2.0$ , the pattern in Fig.6(a) is obtained with values of the temporal mode  $\omega$  and the coefficient of the exponential temporal kernel  $\alpha$ , both chosen such that they lie *above* the Turing-Hopf bifurcation curve in Fig.5(a). The pattern in Fig.6(b) is obtained with values of  $\omega$  and  $\alpha$  chosen *on* this Turing-Hopf bifurcation curve, and the pattern in Fig.6(c) is obtained with the values chosen *below* this Turing-Hopf bifurcation curve.

Comparing the patterns in these panels, one can clearly see that for a total time interval of 10 units, there is a change in the number of temporal oscillations, while the number of spatial oscillations does not change (because the spatial mode is fixed at  $k = 25.0$ ). In Fig.6(a), with the values of  $\omega$  and  $\alpha$  chosen *above* the Turing-Hopf bifurcation curve, the neural field has a relatively high number of temporal oscillations, i.e., 12 oscillations; in Fig.6(b) with  $\omega$  and  $\alpha$  chosen *on* the Turing-Hopf bifurcation curve, the number of oscillations is reduced to 6; and in Fig.6(c), with  $\omega$  and  $\alpha$  chosen *below* the Turing-Hopf bifurcation curve, the number of oscillations is further reduced to 2.

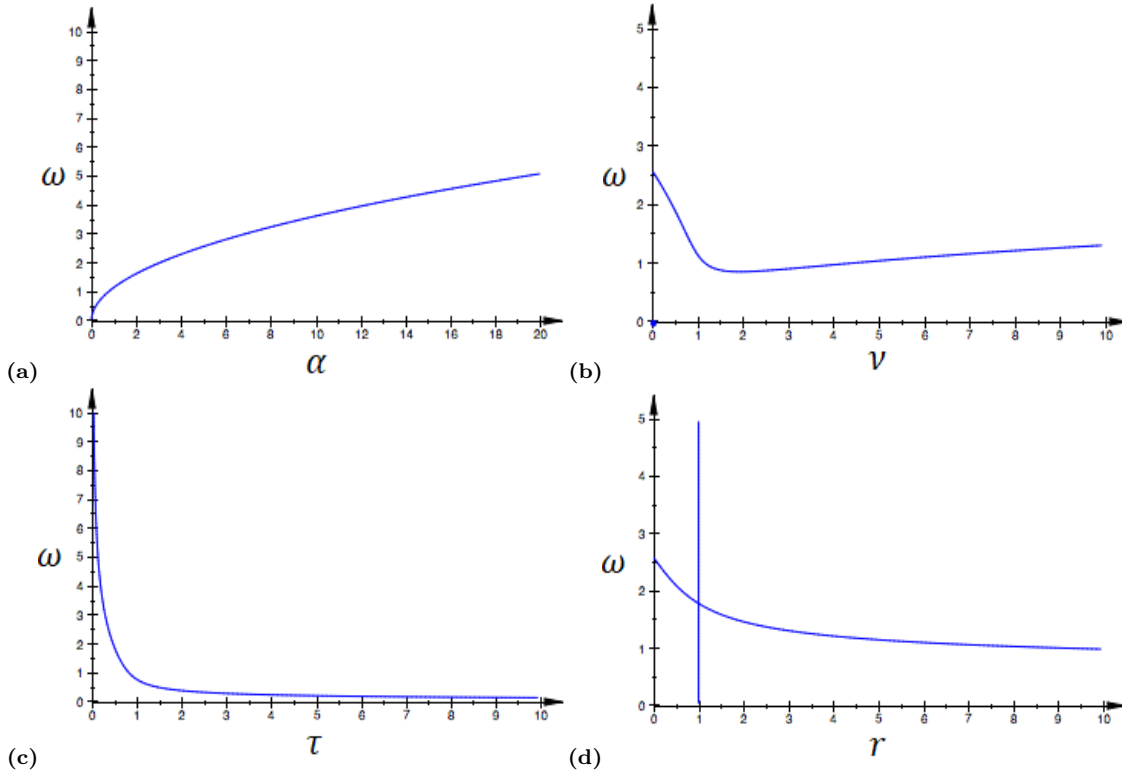


Figure 5: The curves in panels (a)-(d) represent the Turing Hopf bifurcation curves in (5.25) in the  $(\alpha-\omega)$ ,  $(\nu-\omega)$ ,  $(\tau-\omega)$ , and  $(r-\omega)$  planes, respectively. Parameter values are: (a)  $k = 25.0$ ,  $\nu = 1.0$ ,  $\tau = 0.75$ ,  $r = 5.0$ ; (b)  $k = 1.0$ ,  $\alpha = 5.0$ ,  $\tau = 0.75$ ,  $r = 5.0$ ; (c)  $k = 1.0$ ,  $\alpha = 5.0$ ,  $\nu = 1.0$ ,  $r = 5.0$ ; (d)  $k = 1.0$ ,  $\alpha = 5.0$ ,  $\nu = 1.0$ ,  $\tau = 0.75$ . The remaining parameters are fixed at  $a_e = 10.0$ ,  $a_i = a_e/r$ .

In Fig.7(a)-(d), we respectively show the Turing-Hopf bifurcation curves in different parameter spaces:  $(\alpha-k)$ ,  $(\nu-k)$ ,  $(\tau-k)$ , and  $(r-k)$ , for one of the values of the temporal mode (i.e.,  $\omega = 0.1$ ) for which (5.25) has a unique spatial mode solution (i.e.,  $k = 0.897$ ) according to the dispersion relation curve in Fig.4. We should contrast these relations with those of Fig. 5. In effect, the dependence of the temporal and of the spatial frequency values at the bifurcation on those other parameters is essentially opposite. In Fig.8, we display the space-time patterns in three distinct regions of the Turing-Hopf bifurcation curve of Fig.7(a), for example. One can also see, that the Turing-Hopf bifurcation leads to spatially and temporally non-constant solutions. Here, for the sake of comparison, we also fixed the parameters to the same values given in Fig.6, i.e.,  $\nu = 1.0$ ,  $\tau = 0.75$ ,  $r = 5.0$ ,  $a_e = 10.0$ ,  $a_i = a_e/r = 2.0$ , and temporal mode parameter is fixed at  $\omega = 0.1$ . similarly to patterns in Fig.6, the patterns in Fig.8(a) is obtained with values of the spatial mode  $k$  and the coefficient of the exponential temporal kernel  $\alpha$ , both chosen such that they lie *above* the Turing-Hopf bifurcation curve in Fig.7(a). The pattern in Fig.8(b) is obtained with values of  $k$  and  $\alpha$  chosen exactly *on* this Turing-Hopf bifurcation curve, and the pattern in Fig.8(c) is obtained with the values chosen *below* this Turing-Hopf bifurcation curve.

Comparing these panels, one can see a change in pattern already observed in Fig.6, but in terms of the number of spatial oscillations, for a total space interval of 50 units and a temporal mode fixed at  $\omega = 0.1$ . In Fig.8(a),  $k$  and  $\alpha$  are chosen *above* the Turing-Hopf bifurcation curve in Fig.5(a), and the neural field oscillates with a relatively high number of spatial oscillations, i.e., 13 oscillations. In Fig.8(b),  $k$  and  $\alpha$  are chosen *on* the Turing-Hopf bifurcation curve, and the number of spatial oscillation is reduced 8. And in Fig.8(c),  $k$  and  $\alpha$  are chosen *below* the Turing-Hopf bifurcation curve,

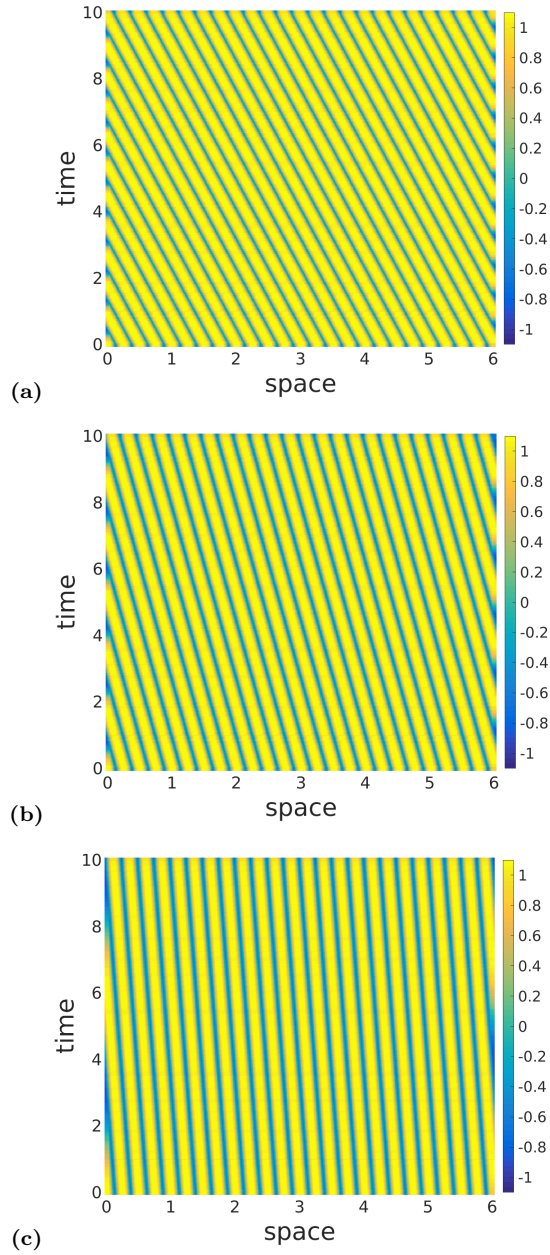


Figure 6: Panels (a)-(c) show color coded space-time patterns of the membrane potential  $v(x, t)$  emerging from a Turing-Hopf instability, leading to periodic oscillations of spatially and temporally non-constant solutions, obtained with the Gaussian connectivity kernel. Initial conditions are chosen randomly from a uniform distribution on  $[v_0 - 0.1, v_0 + 0.1]$ . In panel (a),  $(\alpha, \omega) = (10.0, 1.0)$  lies *above* the Turing-Hopf bifurcation curve of Fig.5(a). In (b),  $(\alpha, \omega) = (10.0, 3.62)$  lies *on* this Turing-Hopf bifurcation curve, and in (c)  $(\alpha, \omega) = (10.0, 7.0)$  lies *below* the curve. We observe an decrease in the frequency of the temporal oscillations of Turing-Hopf patterns from panel (a) to (c), and a constant frequency in the spatial oscillations. Parameter values are:  $a_e = 10.0$ ,  $r = 5.0$ ,  $a_i = a_e/r = 2.0$ ,  $\nu = 1.0$ ,  $\tau = 0.75$ ,  $k = 25.0$ .

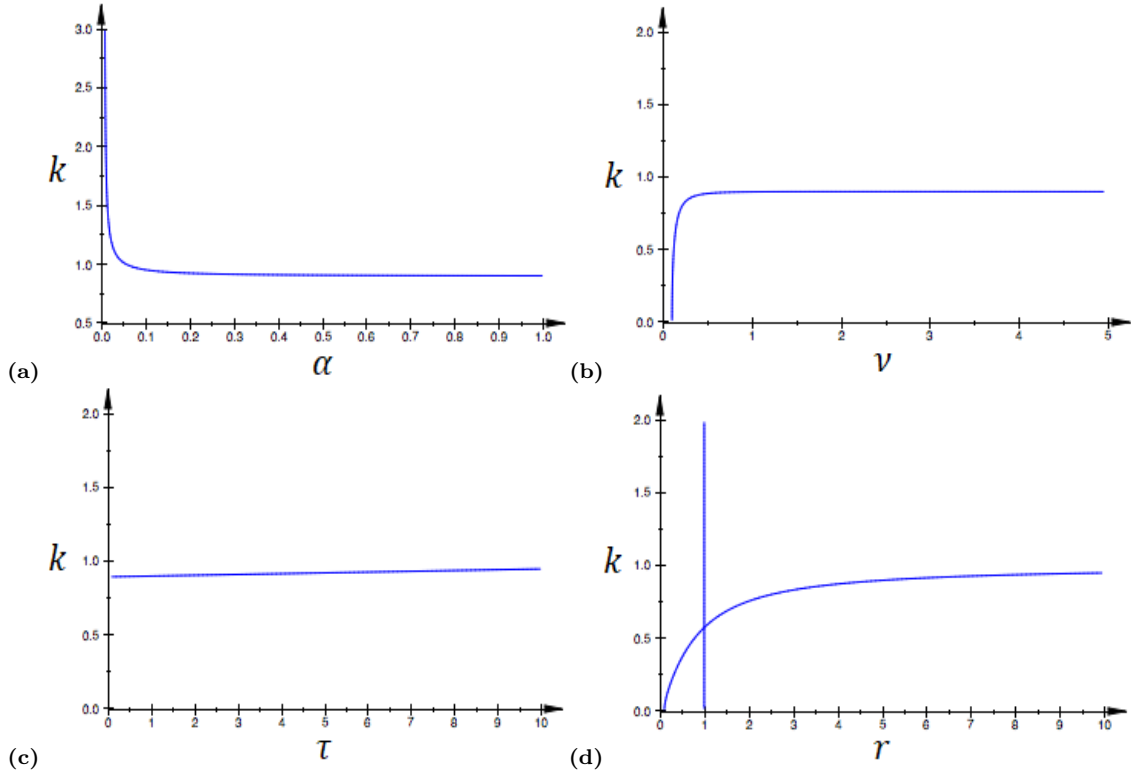


Figure 7: The curves in panels (a)-(d) represent the Turing Hopf bifurcation curves in (5.25) in the  $(\alpha-k)$ ,  $(\nu-k)$ ,  $(\tau-k)$ , and  $(r-k)$  planes, respectively. Parameter values are: (a)  $\omega = 0.1$ ,  $\nu = 1.0$ ,  $\tau = 0.75$ ,  $r = 5.0$ ; (b)  $\omega = 0.1$ ,  $\alpha = 5.0$ ,  $\tau = 0.75$ ,  $r = 5.0$ ; (c)  $\omega = 0.1$ ,  $\alpha = 5.0$ ,  $\nu = 1.0$ ,  $r = 5.0$ ; (d)  $\omega = 0.1$ ,  $\alpha = 5.0$ ,  $\nu = 1.0$ ,  $\tau = 0.75$ . The remaining parameters are fixed at  $a_e = 10.0$ ,  $a_i = a_e/r$ .

and the number of spatial oscillations is further reduced to 5. However, in terms of the wavelengths in both space and time, the space-time patterns of the Turing-Hopf bifurcation in Fig.6 and Fig.8 are different: Fig.8 shows fewer oscillations on larger space and longer time intervals than in Fig.6.

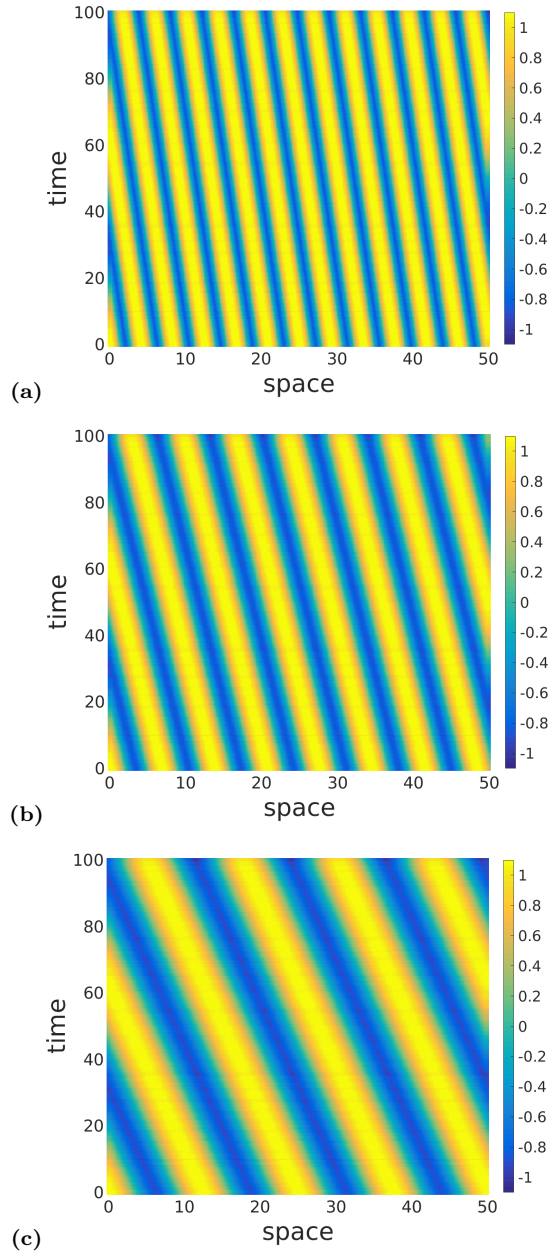


Figure 8: Panels **(a)**-**(c)** show color coded space-time patterns of membrane potential  $v(x, t)$  emerging from Turing-Hopf instability, leading to periodic oscillations of spatially and temporally non-constant solutions, obtained with the Gaussian connectivity kernel. Initial conditions are chosen randomly from a uniform distribution on  $[v_0 - 0.1, v_0 + 0.1]$ . In panel **(a)**,  $(\alpha, k) = (0.5, 0.5)$  lies *above* the Turing-Hopf bifurcation curve of Fig.7**(a)**. In **(b)**,  $(\alpha, k) = (0.5, 0.907)$  lies *on* this Turing-Hopf bifurcation curve, and  $(\alpha, k) = (0.5, 1.5)$  lies *below* this curve. We observe an decrease in the frequency of the spatial oscillations of Turing-Hopf patterns from panel **(a)** to **(c)**, and a constant frequency in the temporal oscillations. Parameter values are:  $a_e = 10.0$ ,  $r = 5.0$ ,  $a_i = a_e/r = 2.0$ ,  $\nu = 1.0$ ,  $\tau = 0.75$ ,  $\omega = 0.1$ .

## 6 Concluding remarks

In this paper we have studied the bifurcation behavior and the wave patterns generated by a neural field equation with an exponential temporal kernel. The exponential temporal kernel in (2.2) takes into account the finite memory of past activities of the neurons, which the Green's function that was utilized in [22] does not.

Our first observation was that static bifurcations such as saddle-node and pitchfork bifurcations, and static Turing patterns are not possible with an exponential temporal kernel, because the characteristic polynomial does not have an eigenvalue 0. This is in contrast to [22], where the temporal kernel was taken as the Green's function rather than an exponential function, and thus allowed zero eigenvalues.

The dynamic bifurcations, however, turn out to be interesting. In the analysis of the dynamic bifurcations of the equilibrium solution, we have obtained the conditions for the occurrence of Hopf and Turing-Hopf bifurcations. Furthermore, we have numerically illustrated these dynamic bifurcations with bifurcation diagrams and space-time patterns.

On one hand, this shows that neural fields can generate rich spatiotemporal patterns. In our analysis, we needed transmission delays and exponentially decaying memory. Both assumptions make sense from a neurophysiological perspective. And on the other hand, these findings support, at least in qualitative terms, neurophysiological models of cognition, like those of [4, 5] and many subsequent ones, that depend on such spatiotemporal patterns.

**Acknowledgements** This work was supported by the Max-Planck-Institut für Mathematik in den Naturwissenschaften, Leipzig, Germany.

## References

1. J.Y.Wu, X.Y. Huang, C. Zhang. Propagating waves of activity in the neocortex: what they are, what they do. *Neuroscientist*. 2008 Oct;14(5):487-502. doi: 10.1177/1073858408317066. PMID: 18997124; PMCID: PMC2679998.
2. Townsend, R.G., Solomon, S.S., Chen, S.C., Pietersen, A.N., Martin, P.R., Solomon, S.G. and Gong, P., 2015. Emergence of complex wave patterns in primate cerebral cortex. *Journal of Neuroscience*, 35(11), pp.4657-4662.
3. Lubenov, E., Siapas, A. Hippocampal theta oscillations are traveling waves. *Nature* 459, 534–539 (2009). <https://doi.org/10.1038/nature08010>
4. von der Malsburg, C. (1981). The correlation theory of brain function. Internal report 81-2, MPI biophysical chemistry. Reprinted in E. Domany, J. L. van Hemmen, & K. Schulten (Eds.), *Models of neural networks II*, chap. 2 (pp. 95–119). Berlin: Springer (1994).
5. Abeles, M. (1982). *Studies of brain function: Vol. 6. Local cortical circuits: An electrophysiological study*. Berlin: Springer.
6. Galinsky VL, Frank LR. Brain Waves: Emergence of Localized, Persistent, Weakly Evanescent Cortical Loops. *J Cogn Neurosci*. 2020 Nov;32(11):2178-2202. doi: 10.1162/jocn-a-01611. Epub 2020 Jul 21. PMID: 32692294; PMCID: PMC7541648.
7. E.R. Kandel, J.H. Schwartz, T.M. Jessell, Department of Biochemistry, Molecular Biophysics Thomas Jessell, S. Siegelbaum, A.J. Hudspeth, *Principles of neural science*, vol 4, McGraw-hill, New York, 2000.
8. H.R. Wilson, J.D. Cowan, A mathematical theory of the functional dynamics of cortical and thalamic nervous tissue, *Biol. Cybernet.* 13 (1973) 55-80.
9. H.R. Wilson, J.D. Cowan, Excitatory and inhibitory interactions in localized populations of model neurons, *Biophys. J.* 12 (1972) 1-24.

10. S.-I. Amari, Dynamics of pattern formation in lateral-inhibition type neural fields, *Biol. Cybernet.* 27 (1977) 77-87.
11. R. Veltz, O. Faugeras, Stability of the stationary solutions of neural field equations with propagation delays, *J. Math. Neurosci.* 1 (2011) 1.
12. L.I. Perlovsky, Toward physics of the mind: Concepts, emotions, consciousness, and symbols, *Phys. Life Rev.* 3 (2006) 23–55.
13. J. Alswaihi, R. Potthast, I. Bojak, D. Saddy, A. Hutt, Kernel reconstruction for delayed neural field equations, *J. Math. Neurosci.* 8 (2018) 3.
14. A.H. Abbassian, M. Fotouhi, M. Heidari, Neural fields with fast learning dynamic kernel, *Biol. Cybernet.* 106 (2012) 15–26.
15. P.C. Bressloff, Spatiotemporal dynamics of continuum neural fields, *J. Phys. A. Math. Theor.* 45 (2011) 033001.
16. H. Haken, *Brain dynamics: an introduction to models and simulations*, Springer-Verlag, Berlin, 2007.
17. J. Karbowski, N. Kopell, Multispikes and synchronization in a large neural network with temporal delays, *Neural Comput.* 12 (2000) 1573-1606.
18. L.G. Morelli, G. Abramson, M.N. Kuperman, Associative memory on a small-world neural network, *Eur. Phys. J. B* 38 (2004) 495-500.
19. T. Prager, L.S Geier, Stochastic resonance in a non-markovian discrete state model for excitable systems, *Phys. Rev. Lett.* 91 (2003) 230601.
20. M. Spiridon, W. Gerstner, Effect of lateral connections on the accuracy of the population code for a network of spiking neurons, *Network* 12 (2001) 409-421.
21. W. Gerstner, W. Kistler, *Spiking neuron models*, Cambridge Univ. Press, 2002
22. F.M. Atay, A. Hutt, Stability and bifurcations in neural fields with finite propagation speed and general connectivity, *SIAM J. Appl. Math.* 65 (2004) 644-666.
23. F.M. Atay, A. Hutt, Neural fields with distributed transmission speeds and long-range feedback delays, *SIAM J. Appl. Dyn. Syst.* 5 (2006) 670-698.
24. A. Hutt, F.M. Atay, Analysis of nonlocal neural fields for both general and gamma-distributed connectivities, *Physica D.* 203 (2005) 30-54.
25. A. Hutt, F.M. Atay, Effects of distributed transmission speeds on propagating activity in neural populations, *Phys. Rev. E* 73 (2006) 021906.
26. J. Senk, K. Korvasová, J. Schuecker, E. Hagen, T. Tetzlaff, M. Diesmann, M. Helias, Conditions for traveling waves in spiking neural networks, arXiv preprint [arXiv:1801.06046](https://arxiv.org/abs/1801.06046)(2018)
27. M. Polner, J.J.W. Van der Vegt, S.V. Gils, A space-time finite element method for neural field equations with transmission delays, *SIAM J. Sci. Comput.* 39 (2017) B797-B818.
28. O. A. Arqub, Adaptation of reproducing kernel algorithm for solving fuzzy fredholm–volterra integrodifferential equations, *Neural Comput. Appl.* 28 (2017) 1591-1610.
29. O. Faugeras, J. Inglis, Stochastic neural field equations: a rigorous footing, *J. Math. Biol.* 71 (2015) 259-300.
30. J. Rankin, D. Avitabile, J. Baladron, G. Faye, D.J. Lloyd, Continuation of localized coherent structures in nonlocal neural field equations, *SIAM J. Sci. Comput.* 36 (2014) B70-B93.
31. J. Fang, G. Faye, Monotone traveling waves for delayed neural field equations, *Math. Models Methods Appl. Sci.* 26 (2016) 1919-1954.
32. M. Breakspear, Dynamic models of large-scale brain activity, *Nat. Neurosci.* 20 (2017) 340.
33. D.J. Pinto and G.B. Ermentrout, Spatially structured activity in synaptically coupled neuronal networks: I. traveling fronts and pulses, *SIAM J. Appl. Math.* 62 (2001) 206-225.
34. S. Coombes, N. Venkov, L. Shiau, I. Bojak, D.T. Liley, C.R. Laing, Modeling electrocortical activity through improved local approximations of integral neural field equations, *Phys. Rev. E* 76 (2007) 051901.

35. A. Hutt, M. Bestehorn, T. Wennekers, Pattern formation in intracortical neuronal fields, *Network* 14 (2003) 351-368.
36. P. A. Robinson, C. J. Rennie, and J. J. Wright, Propagation and stability of waves of electrical activity in the cerebral cortex, *Phys. Rev. E*, 56 (1997), 826-840.
37. S.E. Folias, P.C. Bressloff, Breathers in two-dimensional neural media, *Phys. Rev. Lett.* 95 (2005) 208107.
38. C.R. Laing, Spiral waves in nonlocal equations, *SIAM J. Appl. Dyn. Syst.* 4 (2005) 588-606.
39. S.E. Folias, P.C. Bressloff, Breathing pulses in an excitatory neural network, *SIAM J. Appl. Dyn. Syst.* 3 (2004) 378-407.
40. N.A. Venkov, S. Coombes, P.C. Matthews. Dynamic instabilities in scalar neural field equations with space-dependent delays. *Physica D* 232 (2007) 1-15.
41. J. Touboul, Mean-field equations for stochastic firing-rate neural fields with delays: Derivation and noise-induced transitions, *Physica D* 241 (2012) 1223-1244.
42. I. Bojak, D.T. Liley, Axonal velocity distributions in neural field equations. *PLoS Comput. Biol.* 6 (2010) e1000653.
43. A. Hutt, A. Longtin, L. Schimansky-Geier, Additive noise-induced Turing transitions in spatial systems with application to neural fields and the Swift-Hohenberg equation. *Physica D* 237 (2008) 755-773.
44. S. Coombes, Waves, bumps, and patterns in neural field theories. *Biol. Cybernet.* 93 (2005) 91-108.